Vietnam Journal of Science and Technology ***63*** *(5) (2025) 934-946*

doi:10.15625/2525-2518/18519

Study on solidified material from dredged sediment, fly ash, and blended portland cement using the response surface method

Thai Tien Dat[1, 2, *], Huynh Ngoc Minh[1, 2, *], Luu Tuyen[1, 2], Kieu Do Trung Kien[1, 2], Nguyen Vu Uyen Nhi[1, 2], Do Quang Minh[1, 2]

[1]*Department of Silicate Materials, Faculty of Materials Technology, Ho Chi Minh City University of Technology (HCMUT), 268 Ly Thuong Kiet Street, Dien Hong Ward, Ho Chi Minh City, Viet Nam*

[2]*Vietnam National University Ho Chi Minh City, Linh Xuan Ward, Ho Chi Minh City, Viet Nam*

[*]Emails: *1.ttdat.sdh221@hcmut.edu.vn, 2.hnminh@hcmut.edu.vn*

Received: 14 July 2023; Accepted for publication: 5 March 2024

Abstract. Treating dredged sediment is a complex processing and ongoing challenge. To utilize dredged sediment for the landfill or construction purposes, a material fabricated from a mixture of dredged sediment, Portland cement, and fly ash, was cured under room temperature and hydrothermal condition at 180 °C and 0.9 MPa pressure for 16 hours. The response surface methodology was used to evaluate the compressive strength of the material, with a range of factors investigated including dredged sediment/solids ratio (0.3 - 0.9), cement/fly ash ratio (2 - 4), and water/solids ratio (0.45 - 0.55). The fitting models offered an accurate and reliable match to the actual data. The optimum mix proportions of the two curing conditions were obtained using a total desirability function, meeting multi-objective criteria. This result indicates that hydrothermal curing significantly enhances the treatment capacity of dredged sediment, with a lower CO_2 emission in the mixture compared to ambient curing. Scanning electron microscopy (SEM), X-ray diffraction (XRD), and Fourier transform infrared spectroscopy (FTIR) were used to figure out the difference between the minerals formed in the material under two curing conditions, such as tobermorite.

Keywords: dredged sediment, response surface methodology, solidification, hydrothermal, tobermorite, multi-objective optimization.

Classification numbers: 2.9.4, 2.10.2, 3.4.3.

1. INTRODUCTION

Dredged sediments (DS) include a diverse range of materials from marine dredging operations, continental watercourses, and the erosion of land masses. They consist of fine particles resulting from sediment deposition, introduction of particles into ecosystems, and precipitation of substances through biochemical processes in aquatic environments [1]. The

growing volume of dredged sediments, estimated at approximately 600 Mm^3 annually worldwide [2], presents several challenges, particularly considering their potential pollution and detrimental environmental effects. Consequently, there is a pressing need to identify optimal management approaches for these sediments.

Conventional approaches to managing these sediments involve landfilling and confined or unconfined disposal in the ocean. Nonetheless, these methods have numerous drawbacks, including high costs, limited capacity, and the potential for environmental contamination [3, 4]. Given the substantial quantities of sediments, alternative solutions should be explored to dispose of dredged materials properly.

The application of cementitious materials for stabilization/solidification (S/S) is a well-established and effective method for enhancing the engineering properties of sediments while encapsulating contaminants [5-7]. The process involves incorporating chemical compounds into the dredged material, aiming to achieve two objectives [8]:

(i) chemically immobilizing the contaminants to decrease their leachability and bioavailability,

(ii) geomechanically stabilizing the material to enable its reuse as a new construction material.

Portland cement is widely preferred for stabilization/solidification due to its mechanical properties, widespread availability, and cost-effectiveness. To reduce its environmental effects and improve its mechanical properties, Portland cement (PC) can be partially replaced with pozzolanic materials like fly ash (FA) and ground granulated blast furnace slag (GGBS), etc. [9, 10]. Stabilized/solidified sediment is reused as a construction material instead of depleting other natural resources, which could be used as fill material [11] or bricks [12].

The compressive strength is widely employed as a parameter for assessing the mechanical strength of construction and road materials. In the case of using stabilized/solidified material as a low-strength filling material, the compressive strength should exceed 1.15 MPa after 28 days of maintenance [13]. According to ASTM C62-10 standard, the minimum compressive strength requirement for building bricks is 10.3 MPa, with negligible weathering. Therefore, the compressive strength of treated sediments is the criterion used in the current study.

The coexistence of cement hydration and mineral mixtures affect the kinetics of hydration processes and the mechanisms of microstructure formation, the consequences of which are compressive strength [14]. These effects are further influenced by different curing conditions [15]. The studies conducted by Ribeiro *et al*. [16] and Consoli *et al*. [17] figure out that both the cement dosage and water content play a crucial role in determining the compressive strength values. In addition, the pozzolanic characteristic of FA makes a significant contribution to the improved mechanical performance proven by the compressive strength test with 9 % FA in a mixture of sediments and cement [18]. Further, adding 10 % FA to a mixture of sediments and cement was found to be the most effective in terms of strength [19, 20].

To optimize experimental conditions, the Response Surface Methodology (RSM) is used. It is the optimal solution for giving the response function of many influencing factors at different levels without considering the physical nature of the process. The RSM enables the establishment of functional relationships between influential factors and corresponding response values. By fitting regression equations and visualizing response surfaces and contours, it is easier to identify the response values for each factor level [21]. Additionally, the RSM helps find the best predictors based on the response values at each factor level. Compared to single-factor control methods and orthogonal testing, the RSM offers significant advantages in optimization

design. In recent years, the RSM has also been used to determine the mixing ratio of mortar and concrete [22 - 24].

In this study, the effect of mixture proportions on compressive strength at different curing conditions (hydrothermal and room temperature curing) of solidified materials from PC, DS, and FA was investigated according to the experimental Box-Behnken Design. Response functions are regression equations statistically processed and presented in a graphical form called response surfaces. In addtion to results, the regression equations were processed to determine the maximum DS proportion and minimum PC proportion in the mixture to achieve the compressive strength threshold of concrete brick after 7 days (7.5 MPa) of curing under different conditions.

2. MATERIALS AND METHODS

2.1. Materials

Freshly dredged sediment was gathered from Cai Mep - Thi Vai International Port in Ho Chi Minh City, Viet Nam. Once in the laboratory, the soil was dried at 110 °C for two days. After that, the soil was crushed, ground to under 200 μm, and homogenized.

Cement was a blended Portland cement with brand INSEE, type PCB40, conforming to Vietnamese National Standards TCVN 2682:2020. Clinker content was between 52 to 57 %, limestone was the main natural component of this cement. Fly ash was obtained from Duyen Hai 1 Thermal Power Plant, located in Vinh Long Province, Viet Nam. The fly ash was dried at 110 °C for 24 hours before use.

2.2. Experimental Methods

2.2.1. Response surface methodology (RSM) and statistical analysis

According to some previous studies [18, 25 - 27], the important independent variables affecting the compressive strength of solidified soil and dredged sediment are the type of binder, binder and additive content, soil properties, water content, curing time, etc. However, this study focused on the effects of the DS, PC, FA, and water (W) mixing ratio on compressive strength of solidified dredged sediments by the RSM with the Box-Behnken design. To simplify the number of variables, the ratio DS/(DS+PC+FA), ratio PC/FA, and ratio W/(DS+PC+FA) were selected as independent variables. The two groups of response values correspond to the compressive strength of the curing material at room temperature (y1) and hydrothermal condition (y2) after 7 days(7 d). The coding and non-coding of the three grade variants are presented in Table 1. A total of 15 experimental runs were conducted, with three replicates at the central points.

Table 1. Factors and levels in Box-Behnken design.

Independent variable	Coded symbol	Level		
		-1	0	1
DS/(DS+PC+FA) ratio	x_1	0.3	0.6	0.9
PC/FA ratio	x_2	2	3	4
W/(DS+PC+FA) ratio	x_3	0.4	0.45	0.5

The response surface mix design is presented in Table 2. The models were fitted using regression analysis and analysis of variance (ANOVA), as well as the statistical significance of the quadratic model. The relationship between the response and each variable was visualized through three-dimensional (3D) surface and contour plots using Design Expert 13.0.5.0 software.

Table 2. Design of experimental.

Run	1	2	3	4	5	6	7	8	9	10	11	12	13	14	15
x_1	0.3	0.9	0.3	0.9	0.3	0.9	0.3	0.9	0.6	0.6	0.6	0.6	0.6	0.6	0.6
x_2	2	2	4	4	3	3	3	3	2	4	2	4	3	3	3
x_3	0.45	0.45	0.45	0.45	0.4	0.4	0.5	0.5	0.4	0.4	0.5	0.5	0.45	0.45	0.45

2.2.2. Specimen preparation

To obtain a homogeneous mixture, 100 g of DS, PC, and FA were initially mixed for 1 minute, followed by adding water and an additional mixing period of 4 minutes. The paste mixture was then poured into a cylindrical PVC mold (diameter 21 mm x height 42 mm) and shaken for 2 minutes to remove air voids. To ensure the reliability of the experimental data, three identical samples were prepared for each group. After 48 hours, the samples were disassembled, then divided into two groups. The first group was further cured under room temperature until the desired curing time was reached. The second group was cured under hydrothermal condition (temperature 180 °C, pressure 0.9 MPa) for 16 hours, followed by curing as for the first group.

2.2.3. Specimen testing method

The compressive strength tests were conducted using an electronic universal testing machine (DTU-900 model from Daekyung Tech and Tester). The axial strain was controlled at a rate of 1 mm/min. The force values were measured at the sample failure point or 15 % axial strain. Each compressive strength test was conducted with 3 specimens. The compressive strength results were calculated according to ASTM D2166-16.

After compressive strength tests, representative fragments from fractured surface were selected for microstructure analysis. This analysis was conducted by employing X-ray diffraction (XRD) on EMPYREAN using radiant Cu-Kα (λ = 1.5406 Å). Fourier transform infrared spectroscopy (FTIR) was performed on a NICOLET 6700 with a wavenumber range of 400~4000 cm^{-1} and a resolution of 4 cm^{-1}. Scanning electron microscopy (SEM) observations were carried out using a Hitachi S4800 instrument, with gold-coated specimens.

3. RESULTS AND DISCUSSION

3.1. Response surface design and statistical analysis

The average of the three tests obtained for each experimental combination was fitted to the general form of a quadratic polynomial model. Table 3 presents the results of the experimental design.

Table 3. Results of experimental design.

Run	1	2	3	4	5	6	7	8	9	10	11	12	13	14	15
y_1 (MPa)	7.3	0.89	9.43	1.02	8.87	1.23	7.9	1.04	5.18	5.71	3.18	4.35	5.18	5.76	5.08
y_2 (MPa)	11.49	1.47	12.89	1.71	12.43	1.34	11.12	1.09	9.04	9.98	5.34	6.92	9.33	9.83	9.82

ANOVA performed response fit analysis, regression coefficient estimation, and model significance assessment with statistical software. The adequacy of the model was tested using the F value and the coefficient of determination (R^2). Variables with P-values less than 0.1 are considered valid and with P-values less than 0.05 are considered highly significant [28].

The strength of solidified materials cured under two conditions for 7 d period was analyzed. The quadratic model was found to be fitted and could be adopted because it intuitively reflects the interaction between different variables. The regression model for the coded levels is shown in equations (1) and (2):

$$y_1 = 5.34 - 3.66x_1 + 0.50x_2 - 0.57x_3 - 0.50x_1x_2 + 0.20x_1x_3 + 0.16x_2x_3 - 0.26x_1^2 - 0.42x_2^2 - 0.32x_3^2 \quad (1)$$

$$y_2 = 9.66 - 5.29x_1 + 0.52x_2 - 1.04x_3 - 0.29x_1x_2 + 0.27x_1x_3 + 0.16x_2x_3 - 2.05x_1^2 - 0.72x_2^2 - 1.12x_3^2 \quad (2)$$

The statistics in Table 4 summarize the results of the analysis of variance (ANOVA) of each model. The p-values of all models are less than 0.01, indicating that the regression effect is significant. The p-values for lack of fit are > 0.05 for all models, indicating abnormal errors in the fitted models and a good fit between the measured and predicted values. In addition, the high regression coefficients R^2 (>0.98) show the compatibility of the models, which means that more than 98 % of the experimental data are compatible with the data in the model's predictions. Moreover, the high adjusted regression coefficients adj-R^2 confirm that the model is highly feasible [29]. The contrast between adj-R^2 and pred-R^2 of all fitted models is less than 0.2, which indicates the consistency between adj-R^2 and pred-R^2 [30].

Table 4. ANOVA for response model of experimental results.

	y_1 (MPa)	y_2 (MPa)
Model		
R^2	0.9920	0.9859
Adj-R^2	0.9775	0.9606
Pred-R^2	0.9035	0.7836
F-value	68.55	38.97
p-value	0.0001	0.0004
Lack of fit (p-value)	0.4030	0.0653

Response surface plots can express regression models, including contour and surface plots. They also can directly visualize the combined effects of two factors on the response value, by

keeping other factors at the middle level. Figures 1 and 2 show the response surfaces of the solidified materials at room temperature and under hydrothermal conditions at 7 d.

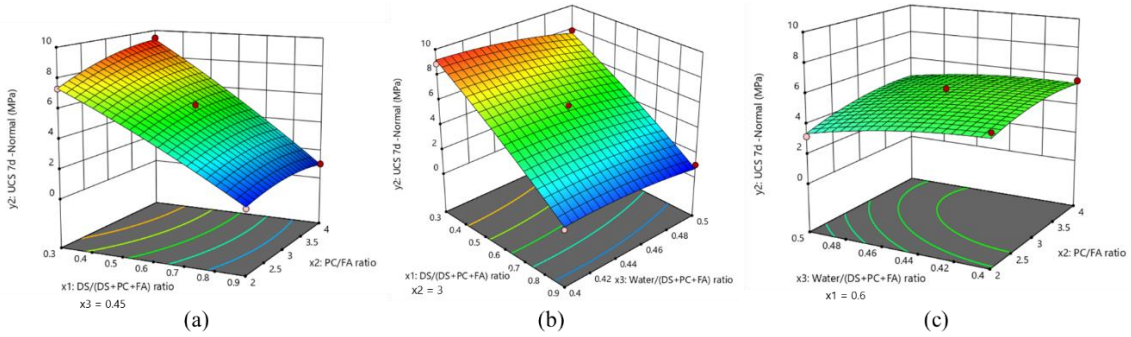

Figure 1. Surface plot for compressive strength of solidified materials at room temperature.

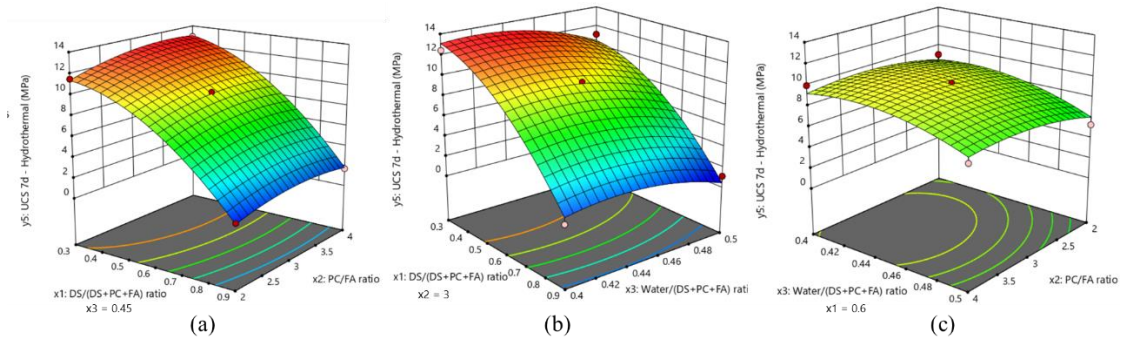

Figure 2. Surface plot for compressive strength of solidified materials under hydrothermal condition.

The effect of the interaction between DS and PC/FA ratios on the compressive strength value can be seen in Figures 1(a) and 2(a). When the ratio of PC/FA remains constant, the compressive strength increases approximately linearly as the DS ratio decreases, the curved surface is steep. At a constant DS ratio, the compressive strength increases with increasing the PC/FA ratio, but it's not a significant change. This indicates that the DS ratio is the main factor influencing material compression strength. The reason is that DS has poor geotechnical properties (low strength and stiffness), a high DS ratio means a low (PC+FA) ratio, that is, the main components have hydraulic activity. A similar result with the interaction between DS ratio and water ratio is also obtained as shown in Figures 1(b) and 2(b).

Figures 1(c) and 2(c) depict the impacts of the PC/FA ratio and water ratio on the compressive strength value, the surface is flat, showing the weak effects of the two factors. The compressive strength value increases when the PC/FA ratio increases for a constant water ratio. If the PC/FA ratio is unchanged, the water ratio will be inversely correlated with compressive strength value.

3.2. Optimizing the proportion of DS in the mixture and applicability

In accordance with the response surface fitting model and the desirability function, the DS ratio, PC/FA ratio, and water ratio are determined to achieve the target compressive strength value at the maximum DS ratio and the minimum PC/FA ratio. Two factors are considered equally important and less important than the target value of compressive strength.

It is defined that the desirability function (d_i) of a single response ranges from 0 to 1, with 0 representing the unsatisfactory response value and 1 representing the response value at the desired level. The total desirability function (D) is the power of each response craving value multiplied exponentially. The goal of multi-objective optimization is to maximize the total desirability function D, which is solved using Design Expert software.

Target values are selected based on technical specifications for concrete blocks according to TCVN 6477:2016. This work uses a strength target of 7.5 MPa at 7 d cured for two conditions. Tables 5 and 6 summarize the optimization criteria and solutions of the two desirability functions, D_1 and D_2.

Table 5. Optimization criteria for different factors, responses, and solutions for the desirability function D_1, compressive strength of materials cured at room temperature at 7 d.

Factor	Goal	Lower limit	Upper limit	Solution
x_1: DS/(DS+PC+FA) ratio	Maximize	0.3	0.9	0.420
x_2: PC/FA ratio	Minimize	2	4	2.609
x_3: Water (W)/(DS+PC+FA) ratio	In range	0.4	0.5	0.400
y_1: compressive strength at 7 d, room temperature curing (MPa)	Target 7.5	0.96	8.99	7.50

As can be seen in Table 5 and Table 6, the optimal ratio obtained with the desirability function value D_1 is 0.754 and D_2 is 0.932, indicating that the projected value is very reliable [29]. In addition, when the specimens were cured under hydrothermal condition, a higher DS ratio and a minimum PC/FA ratio were used for the same compressive strength target compared to room temperature curing condition. This result indicates the positive effect of hydrothermal curing due to the increased DS content and high ratio of PC substituted by FA. This means that CO_2 emissions from the mixture will be significantly reduced and the capacity to process dredged sediments will increase over the same period.

Table 6. Optimization criteria for different factors and responses and solutions for the desirability function D_2, compressive strength of materials cured under hydrothermal condition at 7 d.

Factor	Goal	Lower limit	Upper limit	Solution
x_1: DS/(DS+PC+FA) ratio	Maximize	0.3	0.9	0.666
x_2: PC/FA ratio	Minimize	2	4	2.0
x_3: Water (W)/(DS+PC+FA) ratio	In range	0.4	0.5	0.424
y_2: compressive strength at 7 d, hydrothermal curing (MPa)	Target 7.5	0.98	12.46	7.50

An experiment was performed using these component proportions in mixtures D_1 and D_2 giving results of 7.21 ± 0.11 (MPa) and 7.63 ± 0.08 (MPa) at room temperature and hydrothermal curing conditions, respectively, close to the target value. The model was proved to be validated at these points.

Table 7 shows the CO_2 emissions of the materials in the mixture, assuming the CO_2 emissions of the dredged sediment are close to zero and the proportions of the components in mixtures D_1 and D_2 from are from the above results. The calculated CO_2 emissions in mixtures D_1 and D_2 are 0.127 and 0.066 $kgCO_2/kg$, respectively; the same observation of low CO_2 emissions was reported by Bhairappanavar [31].

Table 7. CO_2 emissions and proportion of components in mixtures D_1 and D_2.

Material	$kgCO_2/kg$	Mixture D_1 (%)	Mixture D_2 (%)
Dredged sediments	/	30.00	46.77
Portland cement	0.419 [32]	29.95	15.64
Fly ash	0.008 [33]	11.47	7.82
Water	0.001 [33]	28.58	29.77

3.3. Microstructure properties

To further investigate the mechanism of mechanical performance, samples were prepared from mixtures with DS ratios of 0.3 and 0.9, PC/FA ratio of 4, and water ratio of 0.45, with specimens in run order 3 and 4, respectively, which were selected for characterization and analysis.

The XRD analysis results of the solidified material samples are presented in Figure 3(a). The occurrence of reaction from cement binder in the mixture under two curing conditions forms new crystalline phases such as ettringite (PDF#41–1451), portlandite (PDF#72–0156), katoite (PDF#77–1713), and tobermorite (PDF#19–1364), which improve the compressive strength performance of the solidified materials. Ettringite, portlandite, and C-S-H gel are the main products of cement hydration. The C-S-H phases exhibit tobermorite or genite structures at the nanoscale, as shown in previous studies [34, 35]. Their structures are characterized by poor crystallinity and short-range properties, which their detection in XRD patterns. Under the hydrothermal curing regime, there are some reactions that change the minerals in the materials. The formation of tobermorite and katoite in 3 – hydrothermal sample through the reaction of portlandite and quartz [36] is shown by the disappearance of the portlandite diffraction peak and the decrease in diffraction intensity in quartz.

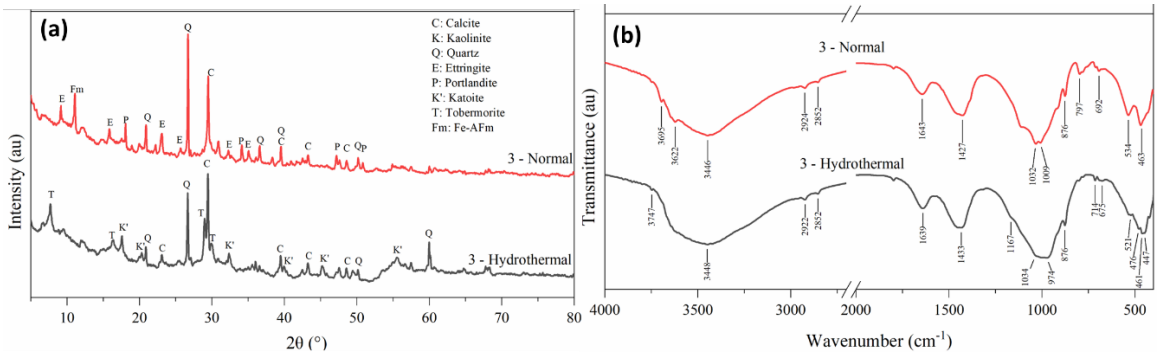

Figure 3. (a) XRD patterns and (b) FTIR spectra of solidified materials.

A similar trend in the FTIR spectra of solidified materials under curing conditions is observed from Figure 3(b). Noteworthy, the FTIR band of sample 3 – Hydrothermal at ~1170 cm^{-1} is characteristic of Al-tobermorite and is assigned to Si-O and/or Al-O stretching of Q_3-silicate (aluminate) tetrahedra [37]. The asymmetric Si-O stretching mode at 970 cm^{-1} indicates the formation of silicate chains containing Q_2 units [38]. This confirms the presence of tobermorite under hydrothermal curing, which is consistent with the XRD results.

Figure 4 show SEM images of the fracture surfaces of the solidified materials under two curing conditions after 7 days. These images confirm the presence of the cementitious component and structural differences due to curing conditions.

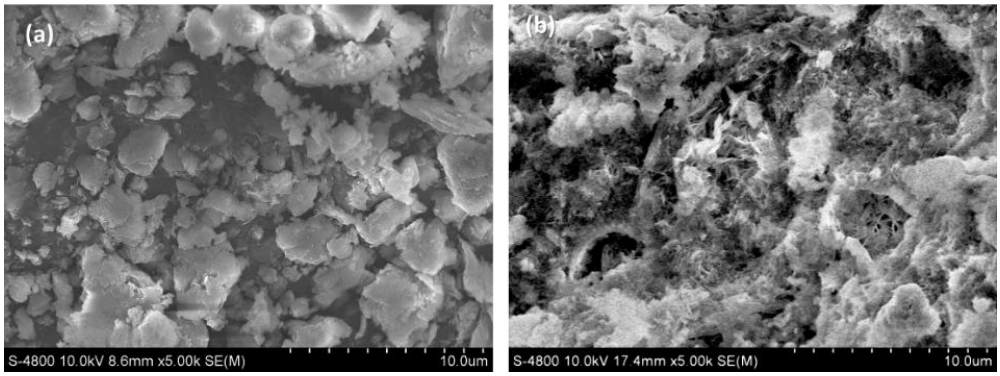

Figure 4. SEM images of (a) 3 – Room temperature sample and (b) 3 – Hydrothermal sample.

Figure 4(a) shows dredged sediments and fly ash particles embedded in the matrixes of gelatinous hydrates with large pores. In Figure 4(b), it can be observed that the sample has a denser structure with fewer pores, and the grain boundaries are more complex than those in Figure 4(a). It reveals the presence of distinct, band-like crystals of tobermorite, approximately 1 μm in size, forming an interlocked honeycomb structure. This result points out the role of tobermorite in enhancing the physical performance of solidified materials by filling the pores with crystalline phase under hydrothermal conditions [39].

4. CONCLUSIONS

In this study, the effects of three variables (DS/(DS+PC+FA) ratio, PC/FA ratio, and W/(DS+PC+FA) ratio) on the compressive strength of solidified materials were investigated using the Response Surface Method according to Box-Behnken design. These models are very compatible, providing a method to design the mixing ratio. The component proportions to achieve a compressive strength of 7.5 MPa in 7 days, while maximizing the DS ratio and minimizing the PC/FA ratio, are as follows: for room temperature curing, 30.0 % DS, 29.95 % PC, 11.48 % FA, and 28.57 % water; for hydrothermal curing, 46.77 % DS, 15.64 % PC, 7.82 % FA, and 29.77 % water. The estimated CO_2 emissions for the mixtures cured at room temperature and under hydrothermal conditions are 0.127 kg CO_2/kg and 0.066 kg CO_2/kg, respectively. Hence, hydrothermal curing presents a promising new treatment method, offering improved processing capacity and increased environmental friendliness.

Characterization of the microstructure of the solidified materials by XRD, FTIR, and SEM analysis showed that hydrothermal curing accelerated the formation of tobermorite, which contributed to the strength improvement by filling the pore spaces.

Acknowledgements. This research is funded by Vietnam National University Ho Chi Minh City under grant number B2024-20-27. We acknowledge Ho Chi Minh City University of Technology (HCMUT), VNU-HCM for supporting this study.

CRediT authorship contribution statement. Thai Tien Dat: Methodology, Investigation, Writing – first draft & Editing. Huynh Ngoc Minh: Supervision, Methodology, Editing. Luu Tuyen: Gathering data, Investigation. Kieu Do Trung Kien: Formal analysis, Manuscript editor. Nguyen Vu Uyen Nhi: Checking

the results, Manuscript review, Visualization. Do Quang Minh: Conceptualization, Writing, Review & Editing.

Declaration of competing interest. The authors declare that they have no known competing financial interests or personal relationships that could have appeared to influence the work reported in this paper.

REFERENCES

1. CapillaX., Schwartz C., Bedell J.P., Sterckeman T., Perrodin Y., andMorel J.L. -Physicochemical and biological characterisation of different dredged sediment deposit sites in France, Environ.Pollut. **143** (2006) 106-116. https://doi.org/10.1016/j.envpol.2005.11.007.
2. Wang D., Abriak N. E., and Zentar R. -Strength and deformation properties of Dunkirk marine sediments solidified with cement, lime and fly ash, Eng. Geol. **166** (2013) 90-99. https://doi.org/10.1016/j.enggeo.2013.09.007.
3. Vinh V. D., Hai N. M., and Lan T. D. -Proposal for appropriate solutions to reduce influences of sediment dumping activities in the Hai Phong open waters, Vietnam J. Mar. Sci. Technol. **19** (2019) 199-213. https://doi.org/10.15625/1859-3097/19/2/12567.
4. Akcil A., Erust C., Ozdemiroglu S., Fonti V., and Beolchini F. -A review of approaches and techniques used in aquatic contaminated sediments: metal removal and stabilization by chemical and biotechnological processes, J. Clean. Prod. **86** (2015) 24-36. https://doi.org/10.1016/j.jclepro.2014.08.009.
5. Barjoveanu G., De Gisi S., Casale R., Todaro F., Notarnicola M., and Teodosiu C. -A life cycle assessment study on the stabilization/solidification treatment processes for contaminated marine sediments, J. Clean. Prod. **201** (2018) 391-402. https://doi.org/10.1016/j.jclepro.2018.08.053.
6. Zhang W., Chen Y., Zhao L., and Chen L. -Mechanical behavior and constitutive relationship of mud with cement and fly ash, Constr. Build. Mater. **150** (2017) 426-434. https://doi.org/10.1016/j.conbuildmat.2017.05.163.
7. Zentar R., Wang H., and Wang D. -Comparative study of stabilization/solidification of dredged sediments with ordinary Portland cement and calcium sulfo-aluminate cement in the framework of valorization in road construction material, Constr. Build. Mater.**279**(2021)122-447.https://doi.org/10.1016/j.conbuildmat.2021.122447.
8. Todaro F., DeGisi S.,andNotarnicola M.-Contaminated marine sediment stabilization/solidification treatment with cement/lime: leaching behaviour investigation, Environ. Sci. Pollut. R. **27** (2020) 21407-21415.https://doi.org/10.1007/s11356-020-085621.
9. Kolias S., Kasselouri-Rigopoulou V., and Karahalios A. -Stabilisation of clayey soils with high calcium fly ash and cement, Cem. Concr. Compos. **27** (2005) 301-313. https://doi.org/10.1016/j.cemconcomp.2004.02.019.
10. Nu N. T., Son B. T., and Hai P. V.-Utilisation of ground granulated blast furnace slag (GGBFS) for soft soil improvement by deep mixing method, J. Min. Earth Sci. **61** (2020) 92-100. https://doi.org/10.46326/JMES.2020.61(1).10.
11. Wang L., Tsang D. C. W., and Poon C.-S. -Green remediation and recycling of contaminated sediment by waste-incorporated stabilization/solidification, Chemosphere **122** (2015) 257-264. https://doi.org/10.1016/j.chemosphere.2014.11.071.

12. Wang L., Yeung T. L. K., Lau A. Y. T., Tsang D. C. W., and Poon C.S. -Recycling contaminated sediment into eco-friendly paving blocks by a combination of binary cement and carbon dioxide curing, J. Clean. Prod. **164** (2017) 1279-1288. https://doi.org/10.1016/j.jclepro.2017.07.070.
13. Ramme B. W. -ACI 229R-99: Controlled Low-Strength Materials, American Concrete Institue (1999), pp. 1-15.
14. Yin B., Kang T., Kang J., Chen Y., Wu L., and Du M. -Investigation of the hydration kinetics and microstructure formation mechanism of fresh fly ash cemented filling materials based on hydration heat and volume resistivity characteristics, Appl. Clay Sci. **166** (2018) 146-158. https://doi.org/10.1016/j.clay.2018.09.019.
15. Zhang K., Wei Q., Jiang S., Shen Z., Zhang Y., Tang R., Yang A. and W. K. Chow C. -Utilization of Dredged River Sediment in Preparing Autoclaved Aerated Concrete Blocks, J. Renew. Mater., **10** (2022) 2989-3008.https://doi.org/10.32604/jrm.2022.019821.
16. Ribeiro D., Néri R. and Cardoso R. -Influence of Water Content in the UCS of Soil-Cement Mixtures for Different Cement Dosages, Procedia Eng., **143** (2016) 59-66. https://doi.org/10.1016/j.proeng.2016.06.008.
17. Consoli N. C., Rosa D. A., Cruz R. C., and Rosa A. D. -Water content, porosity and cement content as parameters controlling strength of artificially cemented silty soil, Eng. Geol. **122** (2011) 328-333. https://doi.org/10.1016/j.enggeo.2011.05.017.
18. Furlan A. P., Razakamanantsoa A., Ranaivomanana H., Amiri O., Levacher D., and Deneele D. -Effect of fly ash on microstructural and resistance characteristics of dredged sediment stabilized with lime and cement, Constr. Build. Mater. **272** (2021) 121637. https://doi.org/10.1016/j.conbuildmat.2020.121637.
19. Jamsawang P., Charoensil S., Namjan T., Jongpradist P., and Likitlersuang S. -Mechanical and microstructural properties of dredged sediments treated with cement and fly ash for use as road materials, Road Mater. Pavement **22** (2021) 2498-2522. https://doi.org/10.1080/14680629.2020.1772349.
20. Yoobanpot N., Jamsawang P., Simarat P., Jongpradist P., and Likitlersuang S. -Sustainable reuse of dredged sediments as pavement materials by cement and fly ash stabilization, Journal of Soils and Sediments **20** (2020) 3807-3823. https://doi.org/10.1007/s11368-020-02635-x.
21. Nguyen P. B. and Dao D. T. A. -Optimization of enzymatic hydrolysis conditions for increasing the efficiency of dry matter extracted from *Limonia acidissima* pulp by combined cellulase -pectinase enzymes using response surface methodology, Vietnam J. Sci. Technol. **55** (2017) 15. https://doi.org/10.15625/0866-708X/55/1/7472.
22. Ahmad M. and Rashid K. -Novel approach to synthesize clay-based geopolymer brick: Optimizing molding pressure and precursors' proportioning, Constr. Build. Mater. **322** (2022) 126472. https://doi.org/10.1016/j.conbuildmat.2022.126472.
23. Li S., Wang D., Tang C., and Chen Y. -Optimization of synergy between cement, slag, and phosphogypsum for marine soft clay solidification, Constr. Build. Mater. **374** (2023) 130902. https://doi.org/10.1016/j.conbuildmat.2023.130902.
24. Srinivasa A. S., Swaminathan K. and Yaragal S. C. -Microstructural and optimization studies on novel one-part geopolymer pastes by Box-Behnken response surface design

method, Case Stud. Constr. Mater. **18** (2023) e01946. https://doi.org/10.1016/j.cscm.2023.e01946.

25. Sridharan A., Prashanth J. P., and Sivapullaiah P. V. -Effect of fly ash on the unconfined compressive strength of black cotton soil, Proceedings of the Institution of Civil Engineers - Ground Improvement,Vol. 4,pp.169-175. https://doi.org/10.1680/gi.1997.010304.
26. Bui T. S., Nguyen T. N., and Nguyen T. D. -An Experimental Study on Unconfined Compressive Strength of Soft Soil-Cement Mixtures with or without GGBFS in the Coastal Area of Vietnam, Adv. Civ. Eng. **2020** (2020) 1-12. https://doi.org/10.1155/2020/7243704.
27. Pham V.N., Oh E., and Ong D. E. L. -Effects of binder types and other significant variables on the unconfined compressive strength of chemical-stabilized clayey soil using gene-expression programming, Neural Comput. Appl. **34** (2022) 9103-9121. https://doi.org/10.1007/s00521-022-06931-0.
28. Kockal N. U. and Ozturan T. -Optimization of properties of fly ash aggregates for high-strength lightweight concrete production, Mater. Des. **32** (2011) 3586-3593. https://doi.org/10.1016/j.matdes.2011.02.028.
29. Shi X., Zhang C., Wang X., Zhang T. and Wang Q. -Response surface methodology for multi-objective optimization of fly ash-GGBS based geopolymer mortar, Constr. Build. Mater., **315** (2022) 125644. https://doi.org/10.1016/j.conbuildmat.2021.125644.
30. Ebrahimzade I., Ebrahimi-Nik M., Rohani A., and Tedesco S. -Higher energy conversion efficiency in anaerobic degradation of bioplastic by response surface methodology, J. Clean. Prod. **290** (2021) 125840. https://doi.org/10.1016/j.jclepro.2021.125840.
31. Bhairappanavar S., Liu R., and Shakoor A. -Eco-friendly dredged material-cement bricks, Constr. Build. Mater. **271** (2021) 121524. https://doi.org/10.1016/j.conbuildmat.2020.121524.
32. Siam City Cement (Viet Nam) Ltd., INSEE Sustainable Development Report 2020-2021 Vietnam, 2022, https://static.insee.com.vn/SUSTAINABLE_DEVELOPMENT_REPORT_2020_2021..pdf (accessed 02 July 2023).
33. Hammond G., Jones C., Lowrie F., and Tse P. -Embodied carbon: the Inventory of Carbon and Energy (ICE), BSRIA, Bracknell, 2011.
34. Skibsted J. and Hall C. -Characterization of cement minerals, cements and their reaction products at the atomic and nano scale, Cem. Concr. Res. **38** (2008) 205-225. https://doi.org/10.1016/j.cemconres.2007.09.010.
35. Allen A. J., Thomas J. J., and Jennings H. M. -Composition and density of nanoscale calcium–silicate–hydrate in cement, Nat. Mater. **6** (2007) 311-316. https://doi.org/10.1038/nmat1871.
36. Galvánková L., Másilko J., Solný T., and Štěpánková E. -Tobermorite Synthesis Under Hydrothermal Conditions, Procedia Eng. **151** (2016) 100-107. https://doi.org/10.1016/j.proeng.2016.07.394.
37. Lothenbach B., Jansen D., Yan Y., and Schreiner J. -Solubility and characterization of synthesized 11 Å Al-tobermorite, Cem. Concr. Res. **159** (2022) 106871. https://doi.org/10.1016/j.cemconres.2022.106871.

38. Mostafa N. Y., Shaltout A. A., Omar H., and Abo-El-Enein S. A. -Hydrothermal synthesis and characterization of aluminium and sulfate substituted 1.1nm tobermorites, J. Alloys Compd. **467** (2009) 332-337. https://doi.org/10.1016/j.jallcom.2007.11.130.
39. Liang X., Wang C., Zhan J., Cui X., and Ren Z. -Study on preparation of eco-friendly autoclaved aerated concrete from low silicon and high iron ore tailings, J. New Mater. Electrochem. Syst. **22** (2019) 224-230. https://doi.org/10.14447/jnmes.v22i4.a08.